Low Frequency Sound Absorption in a Porous Material with Periodically Distributed Dead-End Pores

Philippe Leclaire, Olga Umnova, Thomas Dupont, Raymond Panneton

HAL Id: hal-02558244
https://hal.archives-ouvertes.fr/hal-02558244

Submitted on 25 Sep 2020

Low frequency sound absorption in a porous material with periodically distributed dead-end pores

Philippe Leclaire
DRIVE - ISAT - Universite de Bourgogne, 49, rue Mademoiselle Bourgeois BP31, 58027 Nevers, France.

Olga Umnova
University of Salford, The Crescent, m5 4wt Salford, UK.

Thomas Dupont
DRIVE - ISAT - Universite de Bourgogne, 49, rue Mademoiselle Bourgeois BP31, 58027 Nevers, France.

Raymond Panneton
GAUS, Université de Sherbrooke, Québec J1K 2R1, Canada.

Summary
A theoretical and numerical study of the sound propagation in air-saturated porous media with straight pores bearing lateral cavities (dead-ends) is proposed. The straight pores can be considered as the main (Biot) pores. The lateral cavities are located at "nodes" periodically spaced along each "main pore" axis. The effect of periodicity in the distribution of the lateral cavities is studied and the low frequency limit valid for the closely spaced dead-ends is considered
separately. It is shown that the absorption coefficient and transmission loss are influenced by the viscothermal losses in the main pores as well as their perforation rate. The presence of long or short dead-ends significantly alters the acoustical properties of the material. These depend strongly on the geometry (diameter and length) of the dead-ends, on their number per node and on the periodicity along the propagation axis. These effects are primarily due to low sound velocity in the main pores and on thermal losses occurring in the lateral cavities. The model predictions are compared with experimental results and examples of material design featuring periodically distributed dead-end pores are proposed..

PACS no. 43.50.+y, 43.20.+g

1. Introduction

A model accounting for partially opened or dead-end pores in a material was recently developed [1]. Dead-end pores are closed at one end so that fluid flow does not take place in all the pores of the medium. The characteristic sizes of the pores considered range from a few hundred microns to a few millimeters so that viscous and thermal effects take place at audible frequencies. This model was used to successfully describe the acoustical properties of low porosity materials such as metallic foams and materials with surface dead-end pores. It was found that the presence of dead-ends had the effect of increasing the absorption coefficient at frequencies controlled by the average length of the dead ends.

The present study aims at incorporating an additional feature to the dead-end pores: the fact that these dead-end pores can be periodically distributed along "main pores". The main pores correspond to straight perforation through a material slab while the dead-ends are lateral cavities located at "nodes". This study is motivated by the fact that structured materials with well-controlled microgeometry including dead-end pores can be designed and fabricated by making use of recent technologies such as precision machining or 3D printing. The designed materials slab could contain for example circular perforations. Some of the perforations should go in-through the thickness of the layer (main pores) while others should end inside it in order to create dead-end pores. Theoretical and numerical results are proposed and compared to first experimental results.

Waves propagating in periodic structures are known as "Bloch waves". Examples of such structures are ducts with periodically distributed lateral cavities or resonators (see references [2-4] for example). The periodicity introduces frequency stop bands. Most studies deal with the situation where the period is of the order of the wavelength in order to observe the stop bands (example - sonic crystals). The distances between the perforations and dead-ends considered in the present study are about *1 cm* or less. Therefore, the wavelengths of the order of the period correspond to frequencies above *10 kHz*. However, a stop band due to resonances of the lateral dead-ends are also predicted at low

frequencies, typically a few hundred *Hz*, much lower than the frequencies corresponding to the period. This constitutes the central originality of the present contribution. The dead-end pores considered here are simple closed cavities. However, the model can account for more complex geometries including Helmholtz resonators.

The model presented here provides a simple tool for optimizing the material inner structure to achieve the desired acoustical properties.

2. Analytical and numerical modeling

A periodic arrangement of lateral cavities along a main pore are shown in Figure 1. Only the straight perforations going through the thickness of the material layer are visible on the surface.

When the dead-ends are distributed periodically along the length of the main pores, two distinctive cases can be identified in the material behaviour. If the wavelength of sound travelling through the main pores is comparable to the distance between the dead-ends, stop and pass bands may appear. However, in the small pores of the order of the viscous and thermal boundary layers thicknesses, these effects will be severely affected by the strong viscous and thermal losses. In the case where the separation distance between the dead-ends is much less than the wavelength, the effective properties of the porous material (i.e. its effective density and compressibility) are modified by their presence. The validity of the plane wave approximation is assumed throughout the paper i.e. the radii of all pores are assumed small compared to the wavelength of sound.
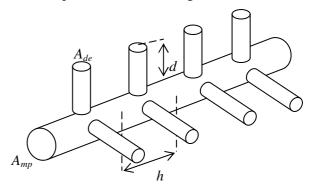

Figure 1. Main pore (cross sectional area A_{mp}) with periodically arranged dead-end pores, *N=2* identical dead-end pores with cross section area A_{de} and length *d* per period *h*. The dead-ends are located at "nodes".

2.1. Pseudo periodic dispersion equation

Following Bradley [2], a pore with cross sectional area A_{mp} (the subscript "mp" stands for "main pore") with periodically distributed identical side branches with cross sectional area A_{de} (the subscript "de" stands for "dead-end") and length d is considered. There are N dead-ends per period h. A configuration with $N=2$ is shown in Figure 1. It is assumed that the main and dead-end pore radii are sufficiently smaller than the wavenumbers so that the waves inside the pores are plane. The period h can be comparable to the wavelength. In this case, the wavenumber q of Bloch waves is defined by the following dispersion equation [2]:

$$\cos(qh) = \cos(k_{mp}h) + iX\sin(k_{mp}h), \quad (1)$$

where k_{mp} is the wavenumber in the main pore and

$$X = -\frac{N}{2}\frac{A_{de}}{A_{mp}}\frac{1}{Zs_{de}}, \quad (2)$$

in which Zs_{de} is the normalised surface impedance of the dead-end

$$Zs_{de} = i\frac{Z_{de}}{Z_{mp}}\cotan(k_{de}d), \quad (3)$$

where k_{de} is the wavenumber in the dead-ends, Z_{mp} and Z_{de} are the characteristic impedances of the main pore and the dead-end, respectively. A time dependence in the form *exp(-iωt)* has been assumed. Contrary to Ref. [2], the difference between the characteristic impedance of air in the main pore and in the dead-end pore is accounted for in Eqs. (3). This difference may arise due to the difference in shape or in cross sectional area of these pores if viscous and thermal losses are present. It is easy to generalize equation (2) for the case of N non-identical dead-end pores per period:

$$X = -\frac{1}{2}\frac{Z_{mp}}{A_{mp}}\sum_{k=1}^{N}\frac{A_{de}^{(k)}}{Z_{de}^{(k)}}\tan\left(k_{de}^{(k)}d^{(k)}\right). \quad (4)$$

In this case, the characteristics of the individual dead-ends are denoted by the superscript *(k)*.

2.2. Transfer Matrix Method (TMM)

If we define

$$y = \exp(ik_{mp}h), \quad (5)$$

then, forward and backward propagating Bloch waves on the right and on the left from the period of size h along the thickness are related by the following matrix:

$$\mathbf{T_c} = \begin{pmatrix} (1+X)y & X \\ -X & \frac{(1-X)}{y} \end{pmatrix}. \quad (6)$$

If n periods are considered, then forward and backward propagating Bloch waves on the right and on the left from this arrangement are related by the matrix:

$$\mathbf{M} = (\mathbf{T_c})^{\mathbf{n}} = \begin{pmatrix} M_{11} & M_{12} \\ M_{21} & M_{22} \end{pmatrix} \quad (7)$$

The expressions for the pressure reflection r_n and transmission t_n coefficients can be determined in terms of the elements of the matrix $\mathbf{M}$ for a main pore bearing n unit periods. The boundary condition at the exit of the last period can be anechoic (open ended) termination or hard back. The former case provides

$$\begin{pmatrix} t_n \\ 0 \end{pmatrix} = \mathbf{M}\begin{pmatrix} 1 \\ r_n \end{pmatrix}, \quad (8)$$

which gives (open ended)

$$r_n = -\frac{M_{21}}{M_{22}} \text{ and } t_n = \frac{1}{M_{22}} \quad (9 \text{ a,b})$$

while for the latter case (hard back), the reflection coefficient is

$$r'_n = \frac{M_{11}-M_{21}}{M_{22}-M_{12}}. \quad (10)$$

To model a material with several adjacent parallel main pores, the perforation rate ϕ is used:

$$\phi = \frac{A_{mp}}{A}. \quad (11)$$

A being the unit cross section incorporating one main pore. In the hard back case, the absorption coefficient of a hard backed slab is calculated by

$$\alpha = 1 - |R'_n|^2 \quad (12)$$

with

$$R'_n = \frac{M'_{11}-M'_{21}}{M'_{22}-M'_{12}}, \quad (13)$$

where M'_{ij} are the elements of a matrix given by

$$\mathbf{M'} = \mathbf{M} \times \mathbf{T} \text{ with } \mathbf{T} = \begin{pmatrix} \frac{1+\phi'}{2\phi} & -\frac{1-\phi'}{2\phi} \\ -\frac{1-\phi'}{2\phi'} & \frac{1+\phi'}{2\phi'} \end{pmatrix}. \quad (14)$$

In the matrix $\mathbf{T}$, the perforation rate ϕ and the coefficient $\phi' = \phi z_0/Z_{mp}$ are used, z_0 being the characteristic acoustic impedance of air.

2.3. Finite Element Modeling (FEM)

Comparisons between the present analytical model, transfer matrix approach (TMM) and virtual measurements obtained with a 3D acoustical FEM simulations using COMSOL software is performed. A main pore with lateral cavities as in Figure 1 is supposed to be inserted in an impedance tube of cross section A (surface area A of Eq. 11). A virtual FEM measurement is then performed on this virtual sample. The three microphones method of ref. [5] is chosen. Parabolic tetrahedral elements are used to mesh the different domains of the tube and an effective fluid of density and bulk modulus given by a model accounting for the shape of the pores. The full TMM model, the FEM or the low frequency asymptotic development in the case of long dead-ends described in the next section can be used to interpret the Bloch dispersion curves featuring stop and pass bands.

3. Low frequency asymptotic expansions

In this section, we consider the case where the period h of the periodic arrangement of the dead-ends is much shorter than the wavelengths. In this case, terms in the pseudo periodic dispersion equation (1) can be expanded to obtained an explicit expression for the Bloch wavenumber q and for the characteristic impedance z of the effective fluid.

The cases of long or short dead-ends with respect to the wavelength can be distinguished. Yet for both cases, $Re(k_{mp}h) \ll 1$ and the configuration with dead-end pores can be replaced by the main pore filled with a fluid described by the effective wavenumber q and the effective impedance z. To derive the expressions for q and z, a simple self-consistent model similar to a coherent potential approximation (CPA) [Ref. 6] is used. In this method, the configuration shown in Figure 1 is replaced by a pore filled with a fluid with still unknown effective properties. Then the following "gedankenexperiment" is performed: if a unit cell of an original periodic arrangement is inserted into this pore, it will not disturb the properties of an effective fluid representing exactly the same periodically arranged unit cells as the inserted one. This implies that if a wave travels through the pore filled with effective fluid, its reflection coefficient from the inserted cell will be 0 and the transmission coefficient will be equal to *exp(iqh)*. In addition, the implicit assumption that the sample is of infinite length or, at least sufficiently long to include many wavelengths is made.

3.1. Long dead-ends

If $Re(k_{mp}h) \ll 1$, the following expressions for the characteristic acoustic impedance and wavenumber of the effective medium are obtained by developing the sine and cosine functions to the first order in the right hand side of Eq. (1). Then it is possible to obtain expressions for the effective density $\rho_e = zq/\omega$ and for the effective compressibility $C_e = q/(z\omega)$ of the fluid in the pore with dead-ends:

$$\rho_e = \rho_{mp}, \tag{15}$$

$$C_e = C_{mp} + C_{de}\frac{NA_{de}}{A_{mp}}\frac{d}{h}\left(\frac{\tan(k_{de}d)}{k_{de}d}\right), \tag{16}$$

where $\rho_{mp} = Z_{mp}k_{mp}/\omega$ and $C_{mp} = k_{mp}/(\omega Z_{mp})$ are the effective density and compressibility of the fluid in the main pore and $C_{de} = k_{de}/(\omega Z_{de})$ is the compressibility of the fluid in the dead-end pores.

It follows that the presence of the dead-end pores does not affect the effective density of the fluid in the main pore. However, it could significantly modify its effective compressibility.

3.2. Short dead-ends

For short dead-ends, in addition to $Re(k_{mp}h) \ll 1$, the assumption $Re(k_{de}d) \ll 1$ is used and the term $\tan(k_{de}d)$ can be further developed at low frequencies ($\tan(k_{de}d) \approx k_{de}d$) in the expressions for the fluid density and compressibility to obtain simple expressions:

$$\rho_e = \rho_{mp}, \tag{17}$$

$$C_e = C_{mp} + C_{de}\frac{V_{de}}{V_{mp}}, \tag{18}$$

where $V_{de} = NA_{de}d$ and $V_{mp} = A_{mp}h$ are the volumes of the dead-ends and the main pore portion per period h of the structure.

4. Model implementation

The densities ρ_{mp} *or* ρ_{de} and compressibilities C_{mp} or C_{de} of the fluid in the main pores or in the dead-ends are needed to model the properties of the Bloch waves. These parameters appear implicitely or explicitely in the full TMM model, in the FEM modeling or in the low frequency asymptotic developments and can be evaluated with the help of a model of equivalent fluid accounting for the complexity of the pore microstructure.

Sound propagation in cylindrical pores with circular cross section with losses in the viscous and thermal boundary layers is known and involves parameters of the cylinders. In this study, it is proposed to use a model of the wave propagation in porous media as these will be able to accommodate for more complex geometries in future works. The Johnson-Champoux-Allard-Lafarge model [7-9] involving 6 parameters has been selected. Other models such as the model by Attenborough [10] could also be used. The 6 parameters involved are the porosity ϕ (related to the perforation rate), the tortuosity α_∞, the flow resistivity σ, the viscous Λ and thermal Λ' characteristic length and the thermal permeability κ' and are given for cylindrical pores in Table I.

The following expressions are used for the effective density and compressibility of fluid in the main and dead-end pores (subscripts "de" and "mp" are omitted in the following two equations):

$$\rho = \rho_0\alpha_\infty\left(1 + \frac{\sigma}{-i\omega\alpha_\infty\rho_0}\sqrt{1 + \frac{-i\omega}{\omega_b}}\right) \tag{19}$$

$$C = \frac{1}{\rho_0 c^2}\left(\gamma - \frac{\gamma-1}{1+\frac{\eta}{-i\omega'\rho_0\kappa'}\sqrt{1+\frac{-i\omega'}{\omega'_b}}}\right) \tag{20}$$

with $\omega' = \omega\sqrt{N_{pr}}$, $\omega_b = \sigma^2\Lambda^2/(4\,\alpha_\infty{}^2\rho_0\eta)$ and $\omega'_b = \Lambda'^2/(4\kappa'^2\rho_0)$ where N_{pr} is the Prandtl number, ρ_0 the air density and η the dynamic viscosity

Table I. Parameters of Johnson-Champoux-Allard-Lafarge model for straight cylindrical pores (subscript "mp") and dead-ends (subscript "de").

$\sigma_{mp,de}$	$\kappa'_{mp,de}$	$\alpha_{\infty mp,de}$	$\Lambda_{mp,de}$	$\Lambda'_{mp,de}$
$\dfrac{8\eta}{a_{mp,de}{}^2}$	$\dfrac{a_{mp,de}{}^2}{8}$	1	$a_{mp,de}$	$a_{mp,de}$

5. Experimental results and comparison with theoretical predictions

In order to validate the theoretical models, a comparison (not displayed here) between the full TMM, FEM and asymptotic developments was carried out first. This simulation has confirmed the consistency of the different approaches.

Experimental results on 3D printed materials with dead-end pores (MP50) studied by Dupont et al. [11] were compared with the model. This sample was built using 3D printing technology. The sample shown in Figure 2 has 4 types of pores. The pore characteristics are listed in Table II. The overall perforation rate of the sample is $\phi=23.4$ %. For this sample, the full TMM model has been modified to account for the 3 types of dead-end pores and for pores without dead ends. Equation (13) has been used to calculate pressure reflection coefficient in the channel associated with each main pore. A uniform distribution of pores at the material surface was assumed. Due to this, the overall perforation rate of the sample was used to calculate the surface area A of the channels. After that the pressure was averaged across the surface of the sample. The comparison between the measurements and the model predictions for the absorption coefficient is shown in Figure 3.
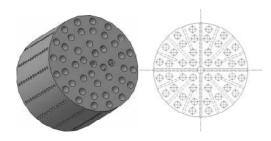

Figure 2. A porous sample with dead-ends (after sealing the circumference) used in the measurements. The sample diameter is 44.4 mm, and its thickness is *L=30 mm.*

Table I. Pore characteristics of the 4 types of pores of the sample presented in Figure 2.

	Pore type 1	Pore type 2	Pore type 3	Pore type 4
Nb of main pores	1	4	8	32
Porosity %	0.52	2.08	4.16	16.62
a_{mp} (mm)	1.6	1.6	1.6	1.6
h (mm)	2.3	2.3	2.3	-
N	4	1	1	-
a_{de} (mm)	0.65	0.65	0.65	-
d (mm)	20.4	15.4	11.4	-

The experimental curve was obtained by averaging 3 sets of results obtained from measurements at different times on 3 identically designed samples in repeatability experiments. The simulation accounts for the end correction of the main pores, which corresponds to a tortuosity correction since the stream lines at the entry face and exit face of the sample are not straight, especially for low perforation rates [12]. The predicted absorption peak is due to the presence of dead-ends. The predicted resonance is broader than the observed one. It is thought that this is due to the fact that the dead-ends in the fabricated sample are slightly thinner than expected in the material design due to the fabrication process. Measuring with precision the actual diameter of the dead-end pores on the fabricated 3D sample is currently a difficult task.
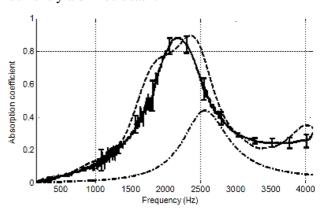

Figure 3. Experimental results on the absorption coefficient for the sample of Figure 2. Experimental results (plain), TMM predictions (dashed) and model predictions for the material without dead-ends (dashed-dot).

However, a simulation using a smaller diameter for the dead-end pores shows that the absorption peak (not displayed here) is narrowed as expected. This provides an indirect confirmation that the pores are thinner than expected. However, the low frequency match is fairly good.

6.   Possible future designs

Future material designs involving periodically spaced dead-ends in the thickness are proposed. The underlying idea is to increase the compressibility at low frequency C_e of the equivalent fluid which can be rewritten

$$C_e = C_{mp} + C_{de} \left(\frac{a_{de}}{a_{mp}} \right)^2 \frac{Nd}{h}, \qquad (21)$$

At constant pore radii, the compressibility can be increased by increasing the number of dead-ends per node N and by reducing the period h. This last condition is compatible with small thickness requirements in the material design. C_e can be increased by increasing the dead-end pore length *d*. An example of possible designs is proposed (Figure 4) with eight dead-ends per node. The perforation rate can be adjusted with the help of additional perforations without dead-ends.
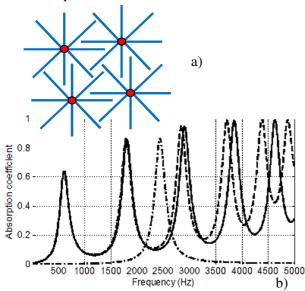

Figure 4. Example of possible design for the front face of a perforated material with lateral dead-ends and b) simulated results. In this example, $N = 8$, $a_{mp} = 2\,mm$, $a_{de} = 1.5\,mm$, $d = 1\,cm$, $h = 3.5\,mm$, slab thickness $L = 3.5\,cm$, perforation rate: $\phi = 5.39\,\%$. Plain curve: low frequency approximation, dashed line: full model, dash-dot line: main pores without dead-ends..

In addition to the sizes of the main pores and of the dead-ends, the criteria for the design are that the material should contain as many dead-ends per nodes as possible while the perforation rate corresponding to the main pores should be chosen optimal. The number of nodes is also important and this parameter indirectly dictates the possible material thickness. Despite the low perforation rate, both materials are efficient absorbers of low frequency sound.

Future more refined optimisation work could include a_{de} and a_{mp} i. e. the pore radii as additional design parameters.

7.   Conclusions

A theoretical and experimental study of the acoustical properties of porous materials containing periodically distributed dead-ends was proposed. This work has shown the great potential of the dead-ends in low frequency applications for materials of only a few cm thicknesses.

With the help of the models developed in this work, it is now possible to design structures giving larger shifts of the absorption coefficient peak towards low frequencies if the Main/DE pores parameters are properly chosen. This opens up new experimental possibilities for future work.

References

[1] T. Dupont, P. Leclaire, O. Sicot, X. L. Gong and R. Panneton: Acoustic properties of air-saturated porous materials containing dead-end porosity. J. Appl. Phys 110 (2011) 094903.

[2] C. E. Bradley: Time harmonic Bloch wave propagation in periodic waveguides. Part I. Theory. J. Acoust. Soc. Am. 96 (1994) 1844-1853.

[3] N. Sugimoto and T. Horioka: Dispersion characteristics of sound waves in a tunnel with an array of Helmholtz resonators. J. Acoust. Soc. Am. 97 (1995) 1446 – 1459.

[4] X. Wang and C. M. Mak: Wave propagation in a duct with a periodic Helmholtz resonators array. J. Acoust. Soc. Am. 131 (2012) 1172 – 1182.

[5] Y. Salissou, O. Doutres, R. Panneton: Complement to standard method for measuring normal incidence with three microphones. J. Acoust. Soc. Am. 131 (2012) EL216.

[6] P. Sheng. Introduction to wave scattering, localization and mesoscopic phenomena, Springer, Berlin, 2006.

[7] D. L. Johnson, J. Koplik and R. Dashen: Theory of dynamic permeability and tortuosity in fluid-saturated porous media. J. Fluid. Mech. 176 (1987) 379-40.

[8] Y. Champoux and J. F. Allard: Dynamic tortuosity and bulk modulus in air-saturated porous media. J. Appl. Phys. 70 (1991) 1975.

[9] D. Lafarge, P. Lemarinier, J. F. Allard and V. Tarnow. Dynamic compressibility of air in porous structures at audible frequencies. J. Acoust. Soc. Am. 102, (1997) 1995.

[10] K. Attenborough: Acoustical characteristics of porous materials. Phys. Rep. 82 (1982) 179-227.

[11] T. Dupont, P. Leclaire and R. Panneton:Acoustic methods for measuring the porosities of porous materials incorporating dead-end pores. J. Acoust. Soc. Am. 133 (2013) 2136 – 2145.

[12] N. Attala and F. Sgard: Modeling of perforated plates and screens using rigid frame porous models. J. Sound Vib. 303 (2007) 195-208.